ISSN 0747-9239, Seismic Instruments, 2016, Vol. 52, No. 3, pp. 195–206. © Allerton Press, Inc., 2016.
Original Russian Text © A.A. Malovichko, I.P. Gabsatarova, M.V. Kolomiets, L.S. Chepkunas, 2015, published in Seismicheskie Pribory, 2015, Vol. 51, No. 3, pp. 5–21.

The Catastrophic Earthquake of April 25, 2015, in Nepal: Analysis of Seismological Data

A. A. Malovichko, I. P. Gabsatarova, M. V. Kolomiets, and L. S. Chepkunas

Geophysical Survey of the Russian Academy of Sciences, pr. Lenina 189, Obninsk, 249035 Russia

e-mail: amal@gsras.ru, ira@gsras.ru, kolmar@gsras.ru, luba@gsras.ru

Abstract—The paper analyzes available seismic data of the Geophysical Survey of the Russian Academy of Sciences on the catastrophic earthquake with *Ms* = 7.9 occurred in Nepal on April 25, 2015. It is shown that this earthquake (also called Gorkha) in its coseismic stage reflected the dynamic situation in the collision zone between the Indian and Eurasian plates, and occurred in the area of the Main Frontal Thrust in the Himalayas. In the last 15 years, the seismicity of this area has demonstrated the features of strong earthquake preparation. The study results are presented for the early postseismic stage (in the first month after the mainshock). It is found that the pattern of a decrease in aftershock activity is similar to that obtained by Tatevossian and Aptekman (2008) for the world's earthquakes with $M > 8$. It is regular in the first 11–16 days and can be described by the Omori law, whereas on 17th day after the mainshock, the exponent characterizing the rate of change in the flow of events becomes to irregular. The spatial and temporal distribution of aftershocks of the 2015 Gorkha earthquake qualitatively and quantitatively indicates the heterogeneity of a seismogenic interface of the Himalayan arc collision zone between the Indian and Eurasian plates.

Keywords: seismicity, Himalayan Seismic Belt, destructive earthquake, focal mechanism, aftershocks

DOI: 10.3103/S0747923916030063

INTRODUCTION

On April 25, 2015, at 06:11 GMT, the strong earthquake with *Ms* = 7.9 occurred in central Nepal. It was one of the catastrophic events of the 21st century that caused multiple deaths and considerable destruction. The previous catastrophic earthquake—Tohoku in Japan (Malovichko et al., 2012)—occurred less than five years ago.

As was reported by Nepalese seismologists, the earthquake epicenter located near the settlement of Barpak in the vicinity of Gorkha area, 76 km northwest of Kathmandu (so that this earthquake is also referred to as Gorkha). Damage was reported in 31 out of 75 administrative subdivisions of Nepal. More than 500 homes, more than 100 historical monuments, numerous schools, hospitals, roads, bridges, water supply systems, hydroelectric power plants, etc, were destroyed.

Based on the data from information agencies, the April 25 earthquake caused more than 9000 deaths and more than 23000 casualties. In Kathmandu, which appeared to be within the VIII shaking zone, massive destruction was reported. Considerable damage was done to the historical center of the city, in particular, the collapse of the 62-m-high Dharahara tower, which was built in 1832 and was a UNESCO World Heritage Site (Fig. 1).

Tremors from this earthquake were felt in adjacent countries, such as China, India, Pakistan, and Bangladesh, with more than 100 casualties reported there.

According to the National Earthquake Information Center (NEIC; http://earthquake.usgs.gov/earthquakes/eventpage/us20002926#general_map) in the United States, the source of the Gorkha earthquake was related to a slip along a sublatitudinal fault. This character of the source caused the formation of an elongated sublatitudinal zone of intensive macroseismic effects on the surface. The zone of manifestations corresponding to I = VII on the Mercalli scale was almost 200 km long and about 75 km wide. The shaking zone with I = VIII was also large; in addition, the shaking zones with I = IX were noted at its northwestern and southeastern ends (Fig. 2).

The epicenter of the strongest aftershock with *Ms* = 7.5 that occurred 17 days after the mainshock was about 100 km from Mount Everest and also caused casualties and destructions. An avalanche hit the base camp, killing 80 climbers (information from TASS).

PARAMETERS OF THE MAINSHOCK OF APRIL 25, 2015

The Earthquake Early Alert Service (EEAS) of the Geophysical Survey of the Russian Academy of Sciences (GS RAS) has processed data from 66 broadband stations of the global seismic network and obtained up-to-date earthquake parameters. The data were from 12 seismic stations located in Russia and from 54 located abroad at the distances of 1800–11300 km from the epicenter (Fig. 3).

Table 1 presents the coordinates of the hypocenter and magnitude of this earthquake, as obtained after

Fig. 1. Aftermaths of earthquakes in Kathmandu: (a) right, ruined Narayana temple and, left, ruined temple on Durbar Square; (b) destroyed Dharahara tower, one of main sights of Nepal (photos from EPA/NARENDRA SHRESTHA and TASS information agencies).

Fig. 2. Map of macroseismic manifestations from earthquake of April 25, 2015, based on NEIC data.

processing at EEAS GS RAS and other leading world seismological centers. Comparison of the different values shows that hypocenter coordinates have been determined with high accuracy (differences of no more than 10 km). The hypocentral depths are also similar, ranging from 13 to 15 km.

DATA ON REGIONAL SEISMICITY AND SEISMOTECTONICS

The epicenter of the analyzed earthquake is located within the Himalayan Seismic Belt (HSB), where the majority of seismic events occurs due to collision between the Indian and Eurasian plates. It has been revealed from geologic and geodetic data (Shah, 2013) that the rate of movement of the Indian Plate toward the Eurasian Plate is 30–50 mm/yr. The active tectonic boundary between the plates where stresses accumulate and then earthquakes occur is the Main Himalayan Thrust (MHT). On the surface, it is expressed as the Main Frontal Thrust (MFT), which is the southern boundary of Himalayas.

For the last 120 years, collision between two plates has led to six large earthquakes with magnitudes of

more than 7.5 that occurred in the Himalayas (Shah, 2013). The epicenters of all these earthquakes (excluding the first in 1897) demonstrate regular migration from west to east along the course of Himalayas: 1905, $M = 7.8$; 1916, $M = 7.5$; 1934, $M = 8.2$; 1947, $M = 7.8$; 1950, $M = 8.4$; and 1897, $M = 8.1$.

One of the last catastrophic earthquakes in Nepal occurred in August 1988; it had a magnitude of $M = 6.9$ and caused 1500 deaths. The epicenter of this earthquake was 240 km southeast of the studied one. The strongest recorded earthquake with $M = 8.2$, also referred to as the Nepal–Bihar earthquake, occurred in nearly the same area in 1934 and resulted in more than 10000 deaths.

The seismotectonic setting of this region has been discussed in a large number of publications, most of which were related to the catastrophic earthquake of January 15, 1934. A detailed list of references has been also compiled by the International Seismological Centre (On-Line Bulletin ..., 2015; Giacomo et al., 2014). Very interesting data on the region have also been presented in a special issue of the Indian interdisciplinary magazine *Current Science* (Monsalve et al., 2006; Kayal, 2014; Mishra, 2014, Kumar et al., 2014, Philip et al., 2014; Jain, 2014; and others).

It was believed for a long time that strong historical earthquakes in this region did not produce ruptures that reached the surface. Supposedly, "blind" earthquakes are caused by sliding on the MFT. This viewpoint changed after the 2005 Kashmir earthquake with $Mw = 7.6$, which caused a nearly 80-km rupture on the surface. The 2005 earthquake spurred studies to rethink and revise the data on ruptures for historical earthquakes in the Himalayas using modern methods.

The first evidence for surface ruptures were obtained from revision of the data on the Bihar earthquake of January 15, 1934, with $Mw = 8.2$. Analysis of paleoseismological data and geomorphologic patterns of river deposits has allowed traces of the rupture to be revealed along at least 150 km of the MFT. In addition, an earlier earthquake was revealed, dated back to June 7, 1255, which also left traces of destruction in this segment of the megathrust.

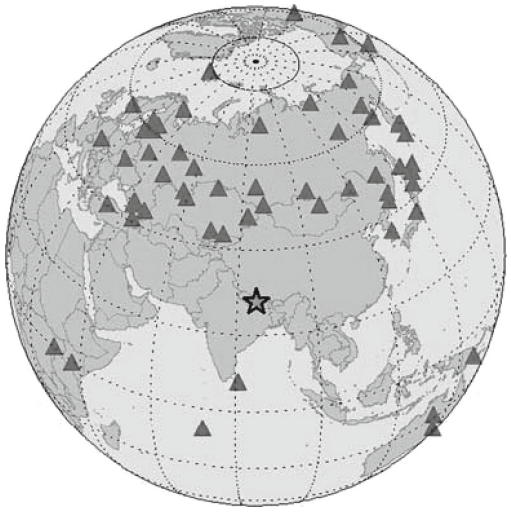

Fig. 3. Seismic stations used by SUR GS RAS to determine coordinates of hypocenter of earthquake of April 25, 2015.

The most widely used seismotectonic model of the HSB implies that catastrophic and strong earthquakes in the Himalayas occur at depths of about 10–20 km (i.e., on the MHT fault plane, which is a detachment plane between the Indian Shield and the Himalayan sedimentary wedge). Nevertheless, recent seismological data (Kayal, 2014) indicate that the seismicity is bimodal in character: the sources are located in both the near-surface layer (0–20 km) and in a layer at a depth of 30–50 km.

The results of contemporary observations also indicate variations in the seismotectonic features along the HSB. Kayal (2014) analyzed the data on the four strongest earthquakes with $Ms \sim 8.0$–8.7 (from west to east): 1905 Kangra, 1934 Bihar, 1897 Shillong, and 1950 Assam; all these events occurred at different tectonic settings.

The 1988 Bihar ($Ms = 6.6$) earthquake that occurred in the foothills of the Himalayas and the 2011 Sikkim ($Mw = 6.9$) earthquake that occurred in the Himalayas proper refer to the zone of deeper sources (~50 km). In contrast to thrust earthquakes, they pos-

Table 1. Comparison of parameters of mainshock of April 25, 2015, based on data from different seismological centers

Source	Time, hh:mm:ss	Latitude, °N	Longitude, °E	Depth, km	Magnitude
GS RAS	06:11:24	28.18	84.78	13	7.9 *Ms*
NEIC	06:11:26	28.15	84.71	15	7.8 *Mw*
IDC (REB)	06:11:24	28.159	84.703	0*	7.8 *Ms*
CSEM	06:11:27	28.24	84.74	15	7.8 *Mw*
BJI	06:11:26	28.20	84.70	20	8.1 *Ms*

Abbreviations of seismological centers: NEIC, National Earthquake Information Center, USGS, United States; IDC, International Data Center of Comprehensive Nuclear Test Ban Treaty Organization (REB bulletin, for which coordinates were determined at fixed depth, $h = 0$ km); CSEM, European–Mediterranean Seismological Centre; BJI, State Seismological Bureau, Beijing, China.

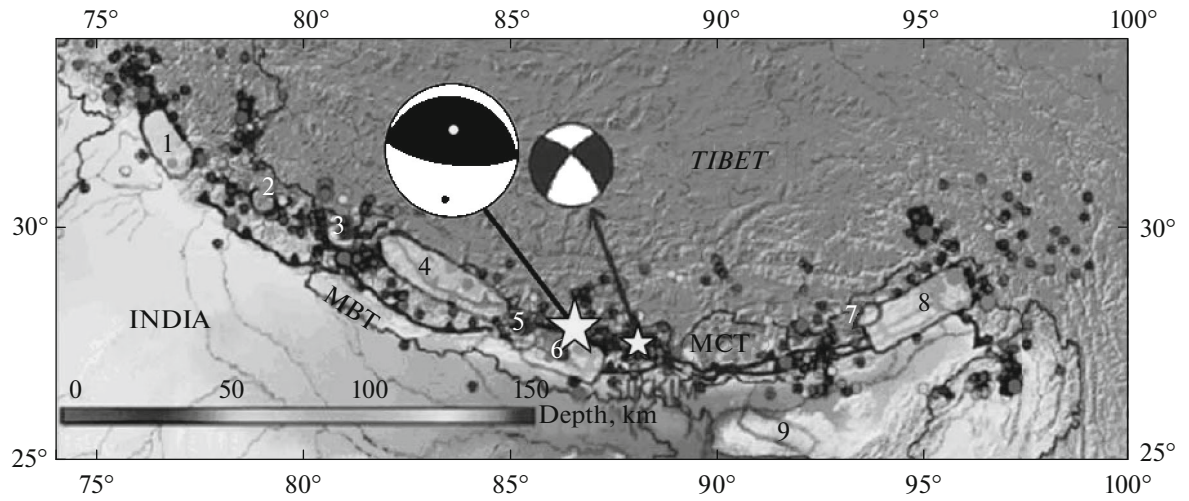

Fig. 4. Map of Himalayan–Tibetan zone with denoted main tectonic structures and earthquakes with $M \geqslant 4.5$. Superimposed gray zones indicate ruptures from main earthquakes of different years in Himalayan region: 1, 1905 ($M = 7.8$); 2, 1803 ($M = 7.3$); 3, 1916 ($M = 7.5$); 4, 1505 ($M = 8.1$); 5, 1833 ($M = 7.3$); 6, 1934 ($M = 8.3$); 7, 1947 ($M = 7.8$); 8, 1950 ($M = 8.4$); 9, 1897 ($M = 8.1$); MBT, Main Boundary Thrust; MCT, Main Central Thrust. Epicenter of 2011 Sikkim earthquake with $Mw = 6.9$ (small star) and its mechanism are after (Mishra, 2014; Philip et al., 2014). The epicenter of earthquake of April 25, 2015, and its mechanism are also indicated.

sessed strike-slip mechanisms. The CMT solutions for both these earthquakes verify that they occurred at greater depths, had strike-slips mechanisms, and were hosted on faults transversely cutting the Himalayas. Study of the aftershock process of the 2011 earthquake by local seismic networks has revealed a vertical structure rooted in the mantle.

Based on detailed seismological observations in Nepal, Monsalve et al. (2006) found the presence of bimodal seismicity. Some earthquake sources were located on the thrust plane, whereas others were hosted in the crustal–mantle zone at greater (40–50 km) depths south and north of the Main Boundary Thrust (MBT) (Fig. 4). Thus, seismic sources in the Himalayas along the MHT are supplemented by sources of mantle dynamics related to dynamic interaction between different segments of the Himalayas.

The geometry of the collisional boundary between the plates in the HSB is wedgelike in shape. The base of this wedge dips north on the MHT. In the west, east, and south, the plate boundaries are marked by other thrusts (Philip et al., 2014), for example, the Main Central Thrust (MCT), MBT, and others (Fig. 5).

Bilham and Ambraseys (2005) carried out a comparative analysis of plate motion rates from seismological and geodetic data. They found that plate motion rates from the total seismic moment due to the release of accumulated elastic energy in the form of the strongest earthquakes in the Himalayan region for 1500–2000 were obviously underestimated in comparison to the same rates calculated from GPS measurements in the last decade. According to these authors, for these rates to match, at least four earthquakes with $M > 8.6$ had to occur, and the contribution of missed historical earthquakes should not exceed 20%.

The study of seismicity prior to the Nepal earthquake based on Global CMT Catalog data (Dziewonski et al., 1981; Ekström et al., 2012) has shown that the most remarkable earthquakes (with $M \geqslant 5.0$) of the last 15 years occurred in the MCT zone, as well as the last one, the Nepal earthquake studied here (Fig. 5).

We can see the effect of alternation of earthquakes between the right and left flanks relative to the area where the earthquake of April 25, 2015, occurred. Within this area proper, rare earthquakes no more than 5.0 in magnitude have been recorded (Table 2, Fig. 5). The number of earthquakes in the left flank is insignificantly greater than that of earthquakes in the right flank, but the right flank zone dominates in terms of magnitudes, with two strong ($M = 6.1$ and $M = 6.9$) earthquakes. In the left flank, epicenters demonstrate migration from west to southeast and the reverse-fault and thrust mechanisms typical for this zone: June 7, 2010; April 7, 2011; August 23, 2012; June 28, 2013; and finally, the earthquake of December 18, 2014 that occurred nearly in the epicentral zone of the future earthquake of April 25, 2015.

Approximately at the same distance from the future epicenter (about 300 km), earthquakes with strike-slip mechanisms occurred in both the left and right flanks on faults running transversely to the main trend of the Himalayas. The depths of sources for the majority of these sources correspond to the lower crust, near the crustal–mantle boundary. For example, an earthquake with a source depth of about 45 km was recorded in the left flank on October 31, 2005, while

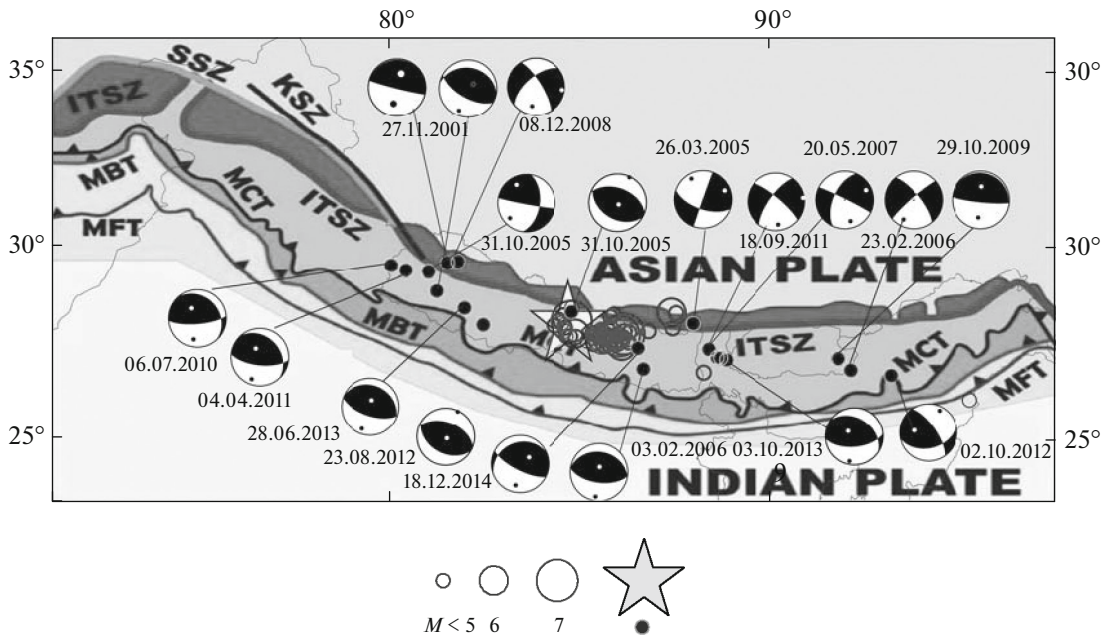

Fig. 5. Tectonic scheme, after (Jain, 2014), with focal mechanisms added (from GCMT catalog for period of 2000–2014). The form of a star denotes mainshock epicenter for Nepal earthquake of April 25, 2015, and circles denote its aftershocks.

six years later, on September 18, 2011, the Sikkim earthquake occurred at almost the same depth.

Thus, the character of seismicity in Nepal during the last 15 years preceding the earthquake of April 25, 2015, allows us to interpret this period as the preparation stage before the strong earthquake in the MCT zone.

DETAILED ANALYSIS OF THE PARAMETERS OF THE MAINSHOCK AND AFTERSHOCKS

Focal Mechanisms

For strong earthquakes, the most reliable focal mechanism parameters can be obtained by analyzing the seismic moment tensor. Below, we use the results of calculations from the Global Centroid Moment Tensor database (http://www.globalcmt.org), known earlier as the Harvard Catalog (Dziewonski et al., 1981) and hereinafter referred to as the GCMT catalog for brevity.

As of May 30, 2015, the GCMT catalog contained data on the mainshock and the strongest aftershocks (Table 3, Fig. 6).

The slip in the mainshock source occurred under the action of compressing stresses from the south, and this agrees with the ideas about the collision between the Indian and Eurasian plates. One gently dipping (DP = 7°) nodal plane, NP1, was west-striking (STK = 293°); the other nearly vertical (DP = 83°)

Table 2. Spatial distribution of epicenters of strong earthquakes in Nepal for last 15 years (based on GCMT catalog)

Left flank			Central zone			Right flank		
date	time	*Mw*	date	time	*Mw*	date	time	*Mw*
27.11.2001	07:31:57	5.5						
31.10.2005	05:51:18	4.7	31.10.2005	21:47:59	4.7			
			03.02.2006	01:57:52	4.7	14.02.2006	00:55:29	5.3
						20.05.2007	14:18:22	4.9
08.12.2008	08:59:12	5.3				21.09.2009	08:53:10	6.1
						29.10.2009	17:00:40	5.1
06.07.2010	19:08:24	5.0						
04.04.2011	11:31:44	5.4				18.09.2011	12:40:59	6.9
23.08.2012	16:30:23	5.0						
28.06.2013	11:40:51	5.0				3.10.2013	06:12:44	4.9
			18.12.2014	15:32:15	5.0			

Dates are in DD.MM.YYYY format; time, hh:mm:ss.

Table 3. Scalar moment M_0, magnitudes on Kanamori scale *Mw*, and parameters of focal mechanisms for mainshock of April 25, 2015 and its strongest aftershocks (based on GCMT catalog)

Date, time	Depth, km	*Mw*	M_0 dyne/cm	T		P		N		NP1			NP2		
				Pl	Azm	Pl	Azm	Pl	Azm	STK	DP	SLIP	STK	DP	SLIP
25.04.2015 6:11:58	12.0	7.9	7.76e+27	52	2	38	187	2	95	293	7	108	95	83	88
25.04.2015 6:45:29	15.8	6.7	1.6e+26	53	344	34	186	10	89	314	14	136	86	80	80
26.04.2015 7:09:22	17.4	6.8	1.76e+26	54	4	35	190	3	98	296	10	108	98	81	87
12.05.2015 7:05:28	12.0	7.2	9.0 e+26	53	356	36	190	7	96	312	11	127	94	81	83
12.05.2015 7:36:59	18.1	6.2	2.29e+25	62	336	25	188	12	92	303	23	123	88	71	77
16.05.2015 11:34:15	12.0	5.4	1.57e+24	61	347	24	201	14	104	318	24	126	99	71	75

Dates are in DD.MM.YYYY format; time, hh:mm:ss.

nodal plane, NP2, was east-trending (STK = 95°). The slip on the subvertical plane was of the reverse-fault type with a left-lateral strike-slip component; the slip on the gently dipping plane was of the thrust type with a right-lateral strike-slip component. The strongest aftershocks inherited the main features of the mainshock mechanism, with a slight increase in the strike-slip component for the aftershocks of May 12 and 16.

The most complete catalog of aftershocks was obtained by the National Seismological Centre in Kathmandu, Nepal (http://seismonepal.gov.np). It is based on the data-processing results from two observation systems: the Regional Seismological Centre at Surkhet, made up of nine stations, and the National Seismological Centre at Kathmandu, made up of 12 stations. As of May 31, 2015, the catalog consisted of 292 earthquakes with $ML \geqslant 4$ (Fig. 7). The aftershock field extended along the Himalayas, with a highly inhomogeneous distribution of aftershocks. Three zones of aftershocks can be distinguished: (1) the western zone located near the mainshock; (2) the central zone in the form of chain consisting of earthquakes with $ML \sim 6$ and cutting the zone in NNE–SSW direction; and (3) the eastern zone characterized by the highest concentration of earthquakes

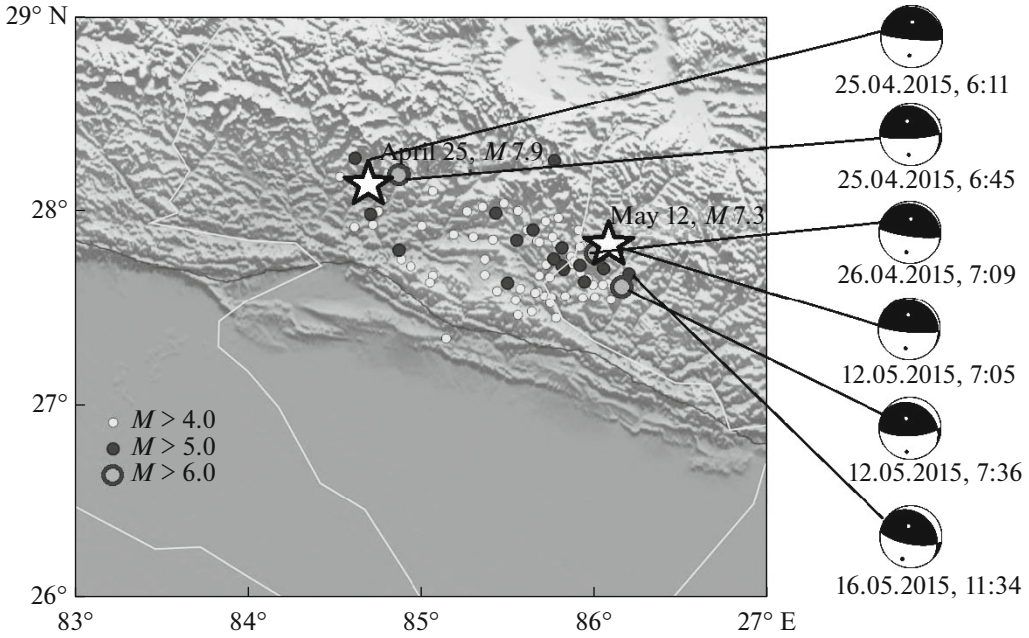

Fig. 6. Epicenters of mainshock of earthquake of April 25, 2015, and its strongest aftershocks based on Indian Seismological Centre (CSIR). Dates and times are in dd.mm.yyyy and hh:mm formats, respectively. Focal mechanisms are from GCMT catalog.

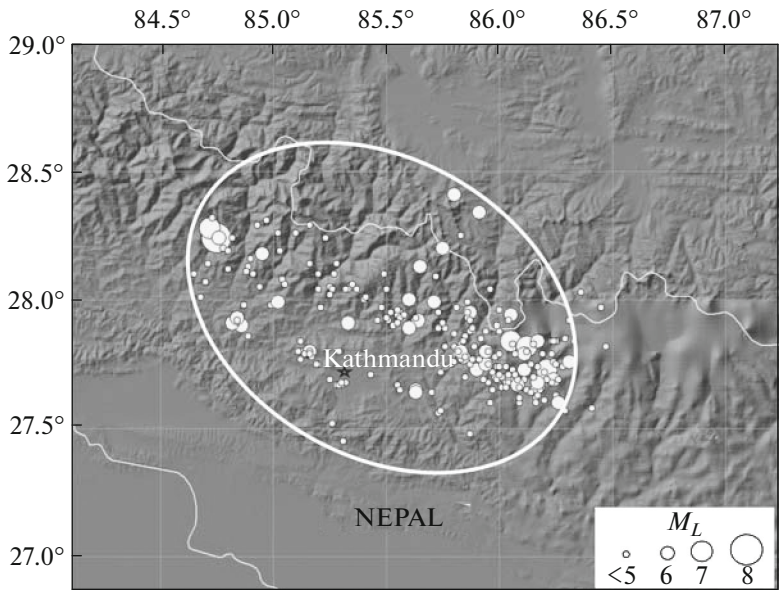

Fig. 7. Aftershock zone of earthquake of April 25, 2015, based on data from National Seismological Centre of Nepal.

around the epicenter of the strongest aftershock that occurred on May 12, 2015. The eastern zone is about 100 km from the mainshock epicenter. The aftershock cloud can be outlined by a NW–SE-elongated ellipse. The major and minor axes are about 160 and 90 km, respectively; the total area is about 10000 km^2.

A quite detailed catalog of aftershocks was also obtained by the State Seismological Bureau, Beijing, China (BJI). As of May 30, 2015, it contained 276 aftershocks with $ML \geqslant 3.0$. This catalog can be accessed through the ISC bulletin (On-Line Event ..., 2015).

Based on the data from EEAS GS RAS, 89 aftershocks with $mb \geqslant 4.5$ were recorded in the first month after the mainshock. It was found that deviations in the positions pf epicenters obtained by EEAS GS RAS from positions obtained by the Nepalese seismological service did not exceed 20 km, on average, indicating the satisfactory accuracy of the technology developed at GS RAS for monitoring of world seismicity.

Spectral and Source Parameters

Using the technique from (Aptekman et al., 1989), we obtained the source spectra of the studied earthquake for the Obninsk and Talaya stations; using the Brune dislocation model, we calculated the dynamic parameters of the source: rupture length L and released stress $\Delta\sigma$. It was found that the interplate earthquake of April 25, 2015, was characterized by a quite large rupture length (L = 108 km) and relatively small released stress ($\Delta\sigma$ = 13–33 bar or 13–33 × 10^5 N/m^2).

For comparison, we present the data on an earthquake with a similar magnitude (Mw = 7.7) and the catastrophic aftermath, but was intraplate in terms of location and occurred in western India on January 26, 2001. As was shown by Negishi et al. (2002), aftershocks of this earthquake covered relatively small area (1260–1960 km^2) which is not characteristic of an earthquake with such a magnitude. However, this earthquake had high value of released stress: $\Delta\sigma$ varied from 126 to 246 bars. Note that the respective value inferred by GS RAS from spectrum obtained at the Talaya seismic station (Zaharova et al., 2007) for the same earthquake was $\Delta\sigma$ = 276 bars.

Thus, the conclusion by Kanamori and Anderson (1975) that intraplate earthquakes usually release larger stresses than interplate ones has been reliably verified by the above comparison.

Interpretation of Source Waves

To study the dynamics of rupture propagation in the source, we analyzed the waveforms from the earthquake of April 25, 2015, recorded by seismic stations located at different azimuths relative to the epicenter. In addition to the Russian stations, those from the Global Seismic Network (GSN) were also involved and accessed through the Wilber-3 system developed by the IRIS corporation.

The direction of rupture propagation can be determined from an azimuthal hodograph (Fig. 8) constructed by the technique from (Gorbunova et al., 1992). This technique is based on the concept of an elongated moving radiation source and investigation of character of source waves in records from stations located at different azimuths relative to the earthquake epicenter. Application of the technique yields an azimuthal hodograph, which is the azimuthal distribu-

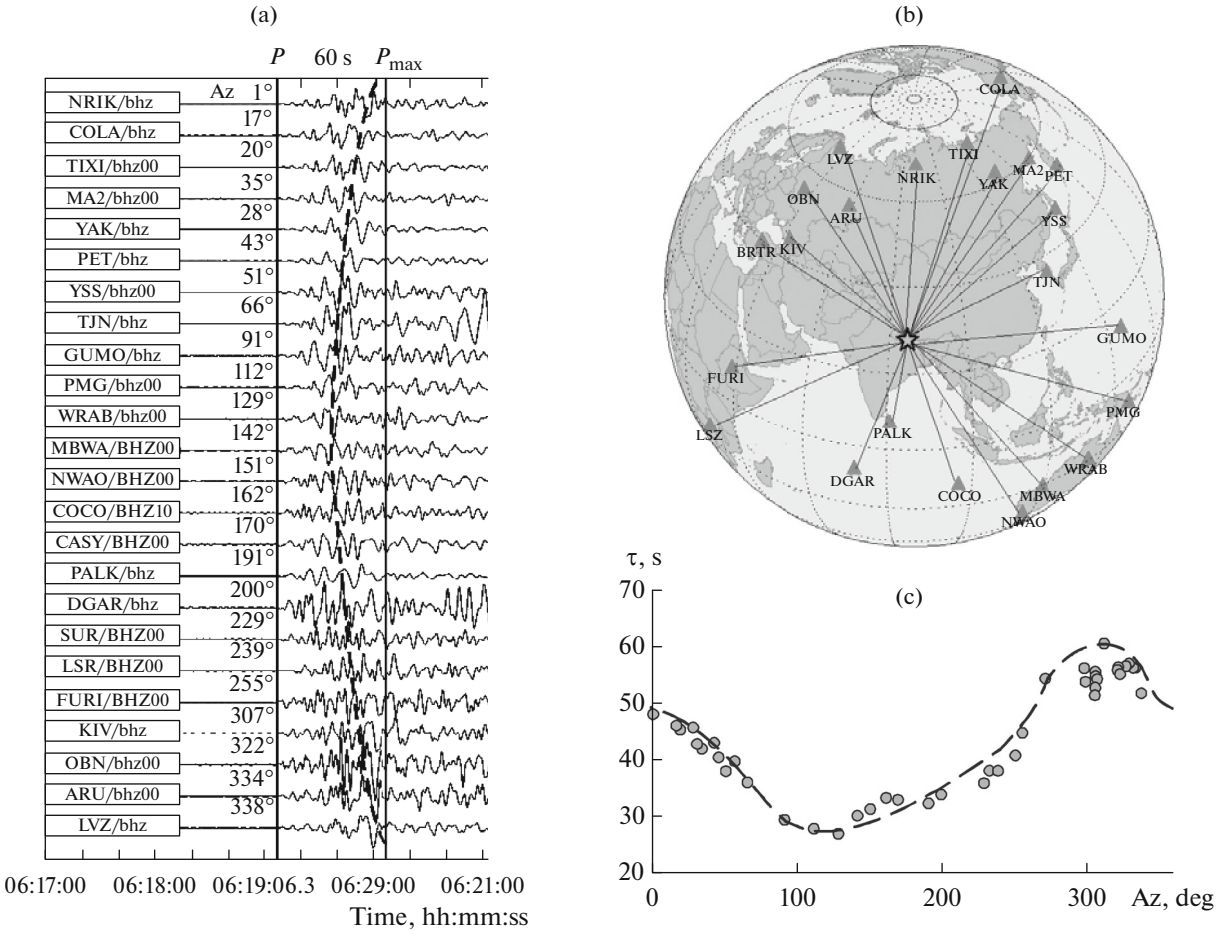

Fig. 8. Fragments of waveforms with maximum amplitudes in group of *P*-waves from earthquake of April 25, 2015 (a), filtered in bandwidth of 0.06–0.2 Hz, at stations at different azimuths (b) relative to epicenter. Panel (c) shows azimuthal hodograph τ.

tion of τ, the delay time of the *P*-wave maximum relative to the first arrival.

A characteristic feature of a source wave is its clear expression in all three record components (Fig. 9). In the case of the strike-slip process, it is expressed more clearly in the horizontal components, while for reverse faulting or thrusting (as in the case of the April 25, 2015 earthquake), it is more noticeable in the vertical component. At close azimuths, source waves are similar, independent of the epicentral distance (Fig. 8a) (Gorbunova et al., 1992).

For the earthquake of April 25, 2015, a source wave is distinguished the most clearly with the application of a Butterworth filter in the 0.06–0.2 Hz bandwidth, which corresponds to periods of 7–15 s.

The azimuthal hodograph of τ for the Nepal earthquake has one clear peak corresponding to a unidirectional rupture in the source. The position of the peak corresponds to azimuths Az = 290°–310°. According to the used technique, the azimuth corresponding to the peak indicates the direction opposite to that of rupture propagation. Hence, rupture propagated at Az = 110°–130°.

The maximum delay time for the *P*-wave maximum is $\tau_{max} = 60.8$ s, while the minimum is $\tau_{min} = 27$ s. In accordance with (Gorbunova et al., 1992), a considerable difference between the τ values for stations of different azimuths indicates a horizontal rupture, because if the rupture were vertical, the azimuthal hodograph would be nearly rectilinear.

An important characteristic of the azimuthal hodograph is the position of its minimum, which is Az = 100°–120° in this case (Fig. 8c).

Upon comparison of the obtained directions of rupture propagation in the azimuthal hodograph and the data on the earthquake focal mechanism, it was noted in (Gorbunova et al., 1992) that the minimum in the azimuthal hodograph corresponds to the direction of the slip vector (SLIP), whereas the maximum in the hodograph determines the strike of one of two nodal planes (STK).

Analyzing the focal mechanism of the Nepal earthquake from the GCMT catalog (first line in Table 2), we can see that parameters of the nodal plane NP1 (STK = 293° and SLIP = 108°), which is a gentle thrust with a right-lateral strike slip component, are

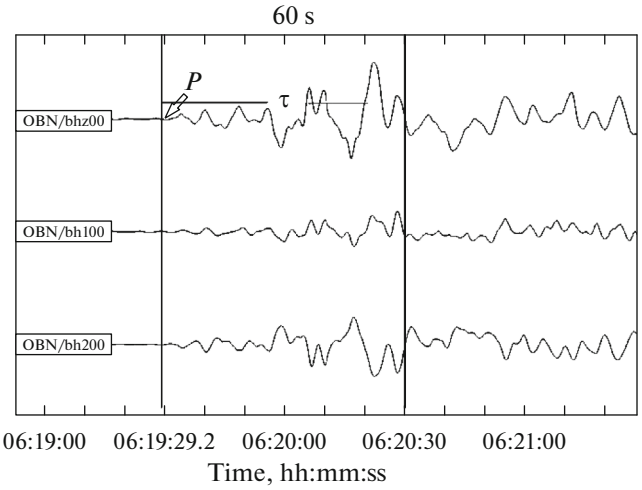

Fig. 9. Fragment of three-component record of first two minutes after first *P*-wave arrival with source wave obtained at Obninsk station for earthquake of April 25, 2015. Record is filtered in bandwidth of 0.06–0.2 Hz.

quite consistent with the values obtained in the azimuthal hodograph.

Using the formulas from (Gorbunova, 1981), let us estimate rupture length L

$$L = \frac{V_P}{2}(\tau_{max} - \tau_{min})$$

and rate of its propagation c

$$c = V_P\left(\frac{\tau_{max} - \tau_{min}}{\tau_{max} + \tau_{min}}\right),$$

where V_P is the longitudinal wave velocity.

Assuming that V_P is 6.6 km/s on average, we obtain $L = 112$ km and $c = 2.54$ km/s.

The found value of the rupture length agrees well with the size of aftershock cloud and is also consistent with the value obtained by spectral analysis of records from the Talaya (TLY) station: $L = 108$ km.

Thus, the rupture of the April 25, 2015, earthquake propagated southeast from the epicenter, and this fits with the direction to Kathmandu ($\varphi = 27.71°$ N, $\lambda = 85.33°$ E). As was shown in (Magnitude..., 2015), the rupture itself ran 20 km north of Kathmandu.

Spatiotemporal Distribution of Aftershocks

Based on the catalog of the National Seismological Centre, which seems the most representative, we analyzed the spatiotemporal distribution of aftershocks by the method of G.A. Sobolev and A.V. Ponomarev (Sobolev, 1993) to reveal possible cluster components of the seismic flow in the epicentral zone of the earthquake. For analysis, we used the EEDB geoinformational system (Mikheeva et al., 2013), where this clusterization method was implemented.

Recall that identification of the cluster component is based on satisfaction of three conditions:

(i) two events s_1 and s_2 are incorporated into the same cluster if their magnitudes are $m_2 \geqslant m_1$;

(ii) the distance between events is $r(s_1, s_2) \leqslant L(s_1) = 3l(s_1)$, where $l(s_1)$ is the rupture length in the source of the event s_1, which empirically depends on the earthquake energy: $l(s_1) = C_e \log E(s_1) + C_l$, usually with $C_e = 0.244$, $C_l = -2.266$ (Riznichenko, 1976);

(iii) the time between events should be $0 < t_2 - t_1 < T(s_1)$, where $T(s_1)$ is the maximum time between events s_1 and s_2.

After analyzing the sampling of aftershocks with $ML \geqslant 5$, we obtained two clusters. The first cluster included the mainshock and aftershocks that occurred in the first hours after the mainshock. It has a small degree of clusterization (–0.125), a total vector azimuth of 129.9°, and a total vector length of 106.6 km. The second cluster included aftershocks from the central "transverse" zone and aftershocks from the east-

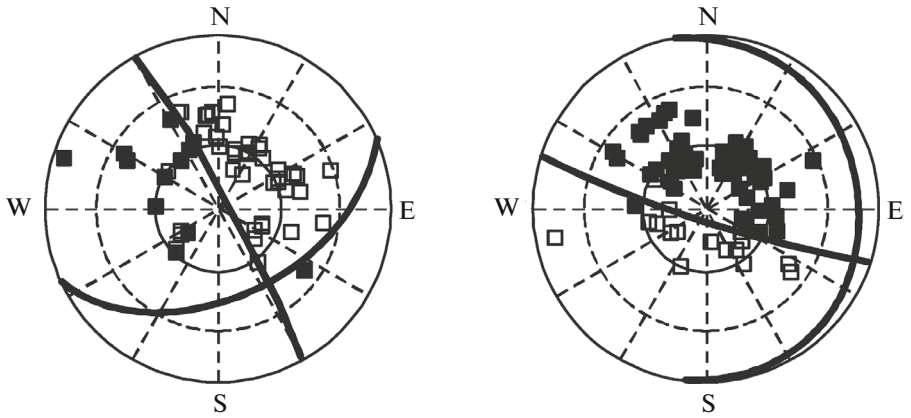

Fig. 10. Distribution of first signs of movement in *P*-wave for aftershocks of Nepal earthquake: left, April 25, 2015, 17:42 min; right, May 12, 2015, 07:05. White and black squares denote – and +, respectively.

Table 4. Parameters of focal mechanism for aftershock of April 25, 2015, 17:42, based on two most probable solutions from *P*-wave signs

mb	T		P		N		NP1			NP2		
	Pl	Azm	Pl	Azm	Pl	Azm	STK	DP	SLIP	STK	DP	SLIP
5.4	32	279	25	26	47	146	65	48	6	331	86	137
	11	287	59	37	28	191	48	42	−45	175	62	−122

ern zone nearest the central one. This cluster has a higher degree of clusterization (−0.875), a total vector azimuth of 172.2°, and a total vector length of 144.4 km.

The result is preliminary, because it was not based on a finite catalog. Nevertheless, it is remarkable for demonstrating the presence of the visually distinguishable transverse zone.

It is interesting that consideration of the records of particular events of this transverse zone has revealed that wave patterns for a number of them differ from the records of events related to typical reverse faults and thrusts. This is particularly expressed in the alternating sign of first motion in the *P*-wave at the most of the stations. For example, Fig. 10 shows the sign distribution in *P*-wave on a Wul'f grid (software by A.V. Lander) and the most probable positions of nodal planes for the aftershock of April 25, 2015 (17:42), which is the northernmost in the transverse zone, and the strongest aftershock of May 12, 2015 (07:05 min), both with reverse-fault or thrust-type mechanisms.

Overlapping of the records from the events, as well as the unavailability of records from the nearest and regional zones, has not allowed us to infer the mechanisms for all aftershocks in the transverse zone based on signs in the *P*-wave at the present stage. In this respect, we can only assume that, in addition to typically reverse faults and thrusts, mechanisms of strike-slip and normal faulting with a strike-slip component could take place in sources, for example, two focal mechanism solutions for the aftershock of April 25, 2015, 17:42 (Table 4), which were the best and equal in terms of statistical estimates.

Deep Phases

For most earthquakes with reverse-fault and thrust types of slips, deep phases *pP* and *sP* have not been successfully distinguished; in contrast, for earthquakes from the supposed transverse zone deep phases, are quite reliably identified in the absence of overlapping related to later quakes (Fig. 11). The difference between the arrival time of deep phase *pP* relative to the first arrival of the *P*-wave (4.13–4.30 s, as obtained for the aftershock of April 25, 2015, 17:42) indicates that the source depth of this aftershock was $h = 13$–14 km in the AK135 hodograph (Kennett et al., 1995).

Tatevossian and Aptekman analysis (2008) of aftershock sequences for several of the world's strongest earthquakes ($Mw \geqslant 8$) has shown that the empirical formulas found earlier are not universally applicable. In particular, the Omori law (Omori, 1894), according to which aftershock activity (number of aftershocks) decreases with time following a regular pattern (more precisely, a power law), and the value of power factor *p* observed in different aftershock series should be close to 1. Tatevossian and Aptekman found that for ten earthquakes in different parts of the world, the Omori law is valid only in a short-term interval at the beginning of their aftershock sequences. The regular character of the decrease in aftershock activity becomes irregular after 7–30 days, and this is often related to the occurrence of a strong aftershock. In their sampling, these two authors did include earthquakes from the collisional zone between the Indian and Eurasian plates. Our study can therefore supplement the list of strong earthquakes with aftershock sequences.

We also studied the character of the change in intensity of the number of aftershocks with time based on the catalog of the National Seismological Centre, which was representative starting from a magnitude of $ML = 4$. As expected, the maximum number of aftershocks ($N = 60$) occurred in the first days, and then the number of diurnal earthquakes decreased (Fig. 12a). If we analyze the entire monthly sampling, it does not satisfy the Omori law ($p = 0.70$ for $r = 0.36$). The process is described well by a power law with a minimum dispersion of points with respect to the regression line—i.e., it agrees with the Omori law—only in the first five days ($p = 1.50$ for $r = 0.99$); in the interval of 6–16 days, dispersion of the points increases¸ but ut still satisfactorily agrees with thw power law ($p = 1.05$ for $r = 0.80$) (Fig. 12b).

On the 18th day after the mainshock, the strongest aftershock with $Mw = 7.2$ occurred on May 12, 2015, at 07:05 min, and interrupted the regularity of the entire seismic flow. However, if we consider the seismic flow day by day after this event, we can see that a regular decrease in number of aftershocks is noticeable starting from the first day after this aftershock (or from the 18th to the 26th day after the mainshock), and the angle of inclination is similar ($p = 1.52$ at $r = 0.95$) to that of the mainshock. The result gives grounds to consider the $Mw = 7.2$ earthquake of May 12, 2015, at 07:05 to be an independent event, but undoubtedly triggered by the first event of April 25, 2015, at 06:11, hosted in the adjacent block divided by the transverse fault.

For comparison, let us provide the empirical dependence of the decrease in aftershock activity for the mentioned catastrophic earthquake of January 26, 2001, in western India. For this study, we used the catalog of central India from the ISC on-line bulletin. Analogous to the Nepal earthquake, let us consider the interval of a month after the mainshock. Figure 12c plots the diurnal variation in the number of aftershocks (in a log–log scale). The maximum number of earthquakes is also observed in the first days after the mainshock ($N = 40$). For the first five days, the process reliably follows with the power law, having the minimum dispersion of points relative to the regression line (i.e., it follows the Omori law; $p = 1.28$ for $r = 0.96$). In the interval of 6–11 days, dispersion increases but still satisfactorily obeys the power law ($p = 0.94$ for $r = 0.85$). After 11 days, the process becomes irregular and contains particular surges.

CONCLUSIONS

The catastrophic $Ms = 7.9$ earthquake of April 25, 2015, in Nepal, which occurred in the zone of the Main Central Thrust in the Himalayas, reflects, at its coseismic stage, the dynamics of the collisional zone between the Indian and Eurasian plates. The seismicity of the last 15 years in this zone has suggested the preparation of a strong earthquake.

The zones of shaking intensities VIII and IX covered a large area of Nepal and led to considerable damage and human casualties.

The mainshock was caused by gentle sublatitudinal thrusting. The rupture length estimated from the constructed azimuthal hodograph was about 110 km.

The earthquake was characterized by an intense aftershock process. Analysis of the spatiotemporal distribution of aftershocks has revealed peculiarities in the

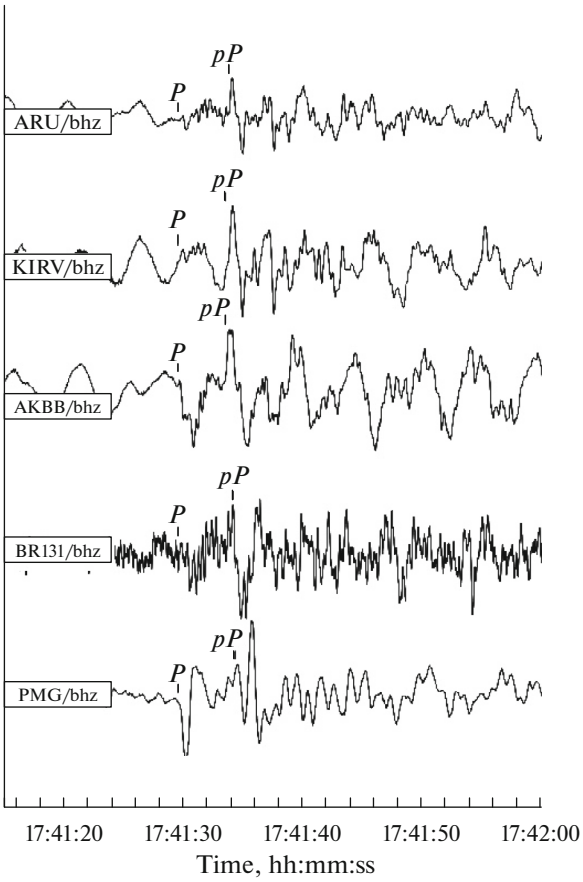

Fig. 11. Deep phases *pP* for aftershock of April 25, 2015, 17:42, as distinguished in nonfiltered records of vertical components of following stations: Arty (ARU), Δ = 34.19°, Az = 333°; Kirov (KIRV), Δ = 39.38°, Az = 331°; central element of Malin array (AKBB), Urkaine, Δ = 47.80°, Az = 314°; element in BRTR array, Turkey (BR131), Δ = 43.43°, Az = 299°); PMG, Δ = 69.90°, Az = 113°. Records are aligned on *P*-wave arrival.

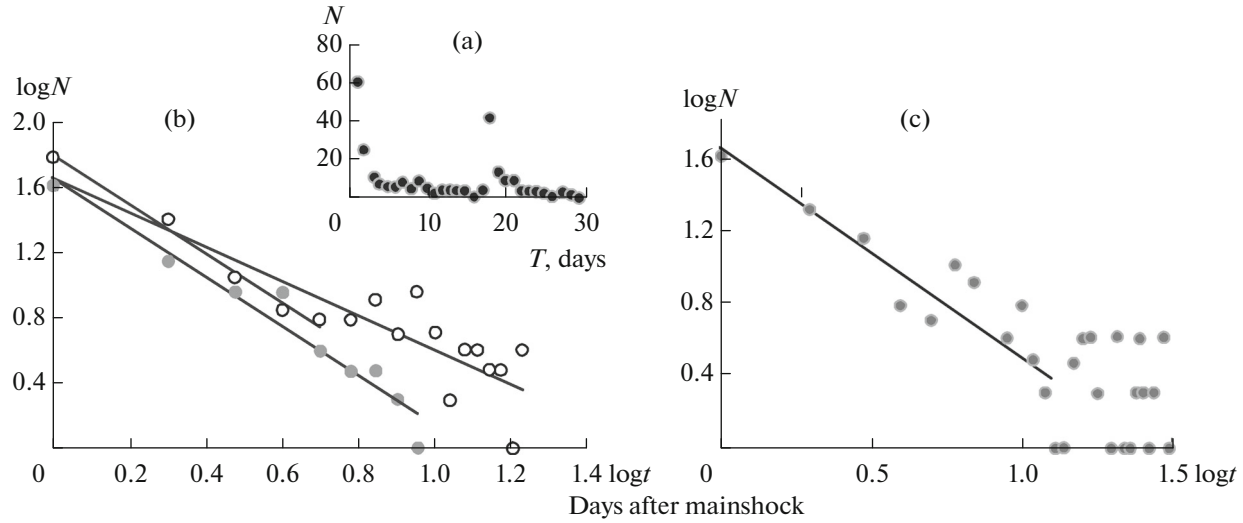

Fig. 12. Diurnal distribution of number of earthquakes in epicentral zones of two strong earthquakes: in Himalayas, April 25, 2015 ((a) linear plot; (b) log–log plot; white circles denote aftershocks of first 17 days; gray circles, day after strong aftershock of May 12, 2015) and in western India, January 26, 2001 (c).

inhomogeneous structure of the Himalayan arc in the collisional zone between the Indian and Eurasian plates.

ACKNOWLEDGMENTS

The work was supported in part by the Russian Foundation for Basic Research (project no. 13-05-00158).

REFERENCES

Aptekman, Zh.Ya., Belavina, Yu.F., Zakharova, A.I., Zobin, V.M., Kogan, S.Ya., Korchagina, O.A., Moskvina, A.G., Polikarpova, L.A., and Chepkunas, L.S., P-wave spectra in the problem of defining the dynamic parameters of earthquakes: A transition from station to source spectrum and calculation of source dynamics parameters, *Vulkanol. Seismol*, 1989, no. 2, pp. 66–79.

Bilham, R. and Ambraseys, N., Apparent Himalayan slip deficit from the summation of the seismic moments for Himalayan earthquakes, 1500–2000, *Current Sci.*, 2005, vol. 88, no. 10, pp. 1658–1663.

Di Giacomo, D., Storchak, D.A., Safronova, N., Ozgo, P., Harris, J., Verney, R., and Bondár, I., A new ISC service: The bibliography of seismic events, *Seismol. Res. Lett.*, 2014, vol. 85, no. 2, pp. 354–360.

Dziewonski, A.M., Chou, T.-A., and Woodhouse, J.H., Determination of earthquake source parameters from waveform data for studies of global and regional seismicity, *J. Geophys. Res.*, 1981, vol. 86, pp. 2825–2852.

Ekström, G., Nettles, M., and Dziewonski, A.M., The global CMT project 2004-2010: Centroid-moment tensors for 13,017 earthquakes, *Phys. Earth Planet. Inter.*, 2012, vols. 200–201, pp. 1–9.

Gorbunova, I.V., Determination of source dimensions and rupture direction from the wave pattern in a seismogram, *Dokl. Akad. Nauk SSSR*, 1981, vol. 261, no. 4, pp. 836–839.

Gorbunova, I.V., Boichuk, A.N., Dotsev, N.T., Kal'met'eva, Z.A., Kapitanova, T.A., Kuchai, O.A., Mikhailova, N.N., Pustovitenko, B.G., Simbirtseva, I.G., and Tovmasyan, A.K., *Interpretatsiya ochagovykh voln na zapisyakh zemletryasenii* (Interpretation of Source Waves in Earthquake Records), Moscow: Geofiz. Kom. Prezidente Ross. Akad. Nauk, 1992.

Jain, A.K., When did India–Azia collide and make the Himalaya?, *Current Sci.*, 2014, vol. 106, no. 2, pp. 254–266.

Kanamori, H. and Anderson, D.L., Theoretical basis of some empirical relations in seismology, *Bull. Seismol. Soc. Am.*, 1975, vol. 65, pp. 1073–1095.

Kayal, J.R., Seismotectonics of the great and large earthquakes in Himalaya, *Current Sci.*, 2014, vol. 106, no. 2, pp. 188–197.

Kennett, B.L.N., Engdahl, E.R., and Buland, R., Constraints on seismic velocities in the Earth from travel times, *Geophys. J. Int.*, 1995, vol. 122, pp. 108–124.

Kumar, M.R., Hazarika, P., Prasad, G.S., Singh, A., and Saha, S., Tectonic implications of the September 2011 Sikkim earthquake, *Current Sci.*, 2012, vol. 102, no. 5, pp. 788–792.

Lander, A.V., *Opisanie i instruktsiya dlya pol'zovatelya kompleksa programm FA (raschet i graficheskoe predstavlenie mekhanizmov ochagov zemletryasenii po znakam pervykh vstuplenii R-voln)* (Description and User Manual of the FA Software Complex: Calculation and Graphical Representation of Focal Mechanisms of Earthquakes from Signs of R-waves First Arrivals), Moscow, 2006.

Magnitude 7.8 NEPAL Saturday, April 25, 2015 at 06:11:26 UTC, Teachable Moments, IRIS Education & Public Outreach, The University of Portland, 2015. http://www.iris.edu/hq/retm/

Malovichko, A.A., Starovoit, O.E., Gabsatarova, I.P., Kolomiets, M.V., and Chepkunas, L.S., Catastrophic Tohoku earthquake of March 11, 2011, in Japan, *Seism. Instrum.*, 2012, vol. 48, no. 1, pp. 1–9.

Mikheeva, A.V., Dyad'kov, P.G., and Marchuk, A.G., The GIS-EEDB geoinformation system and methods of spatio-temporal analysis of seismological data, *Geoinformatika*, 2013, no. 2, pp. 58–65.

Mishra, O.P., Intricacies of the Himalayan seismotectonics and seismogenesis, need for integrated research, *Current Sci.*, 2014, vol. 106, no. 2, pp. 176–187.

Monsalve, G., Sheeha, A.F., Schulte-Pelkum, V., Rajaure, S., Pandey, M.R., and Wu, F., Seismicity and 1-D velocity structure of the Himalayan collision zone: Results from the Himalayan Nepal Tibet Seismic Experiment (HIMNT), *J. Geophys. Res.: Solid Earth*, 2006, vol. 111, B10301.

Negishi, H., Mogi, J., Sato, T., Singh, R., Kumar, S., and Hirata, N., Size and orientation of the fault plane for 2001 Gujarat from aftershock observations: A high stress drop event, *Geophys. Res. Lett.*, 2002, vol. 29, no. 20, pp. 101–104.

Omori, F., Investigation of aftershocks, *Rep. Earthquake Invest. Comm.*, 1896, no. 2, pp. 103–139.

On-Line Bulletin, International Seismological Centre, Thatcham, United Kingdom. http://www.isc.ac.uk/iscbulletin/search/bulletin/. Accessed May 30, 2015.

On-line Event Bibliography, International Seismological Centre, Thatcham, United Kingdom, 2015. http://www.isc.ac.uk/event_bibliography.

Philip, G., Suresh, N., and Bhakuni, S.S., Active tectonics in the northwestern outer Himalaya: evidence of large-magnitude paleoearthquakes in Pinjaur Dun and the Frontal Himalaya, *Current Sci.*, 2014, vol. 106, no. 2, pp. 211–222.

Riznichenko, Yu.V., Source size for a crustal earthquake and seismic moment, in *Issledovaniya po fizike zemletryaseniya* (Studies in Earthquake Physics), Moscow: Nauka, 1976, pp. 9–27.

Shah, A.A., Two great historical earthquake ruptures revealed in Nepal, *Current Sci.*, 2013, vol. 104, no. 8, p. 994.

Sobolev, G.A., *Osnovy prognoza zemletryasenii* (Fundamentals of Earthquake Prediction), Moscow: Nauka, 1993.

Tatevossian, R.E. and Aptekman, Zh.Ya., Aftershock sequences of the strongest earthquakes of the world: Stages of development, *Izv., Phys. Solid Earth*, 2008, vol. 44, no. 12, pp. 945–964.

Zakharova, A.I., Chepkunas, L.S., and Malyanova, L.S., Source parameters of the strong earthquakes of the world, in *Zemletryaseniya Severnoi Evrazii v 2001 godu* (Earthquakes of Northern Eurasia in 2001), Obninsk: GS RAN, 2007, pp. 281–286.

Translated by N. Astafiev